

Chapter 1

Confined Crystals on Substrates: Order and Fluctuations in Between One and Two Dimensions

K. Binder, Y.H. Chui, P. Nielaba, A. Ricci, and S. Sengupta

Abstract The effect of lateral confinement on a crystal of point particles in $d = 2$ dimensions in a strip geometry is studied by Monte Carlo simulations and using phenomenological theoretical concepts. Physically, such systems confined in long strips of width D can be realized via colloidal particles at the air–water interface, or by adsorbed monolayers at suitably nanopatterned substrates, etc. As a generic model, we choose a repulsive interparticle potential decaying with the twelfth inverse power of distance. This system has been well studied in the bulk as a model for two-dimensional melting. The state of the system is found to depend very sensitively on the boundary conditions providing the confinement. For corrugated boundaries commensurate with the order of the bulk (i.e., a triangular crystalline lattice structure), both orientational and positional orders are enhanced, and near the boundaries surface-induced order persists also at temperatures where the system is fluid in the bulk. For incommensurate corrugated boundaries, however, soliton staircases near the boundaries form, causing a pattern of standing strain waves in the strip. However, smooth unstructured repulsive boundaries enhance orientational order only, positional long-range order is destroyed. The strip then exhibits a vanishing shear modulus. A comparison with surface effects on phase transitions in simple Ising and XY -models is also made. Finally, possible applications are discussed.

1.1 Introduction

The research that is briefly reviewed here has three main motivations:

- (i) Colloidal systems allow to carry out experiments of unprecedented detail, comparable to computer simulations: by confocal microscopy techniques, one can

K. Binder (✉)

Institute of Physics, Johannes Gutenberg-Universität, Staudinger Weg 7,

D-55099 Mainz, Germany

e-mail: kurt.binder@uni-mainz.de

provide “snapshot pictures” of all the positions of the colloidal particles; by fluorescent labeling one can track down the motion of arbitrarily selected particles with time; by suitable choice of solvent, and surface treatment of the particles, inter-particle forces are tunable to a large extent: thus, such systems are model systems allowing to study order and disorder in condensed matter in much greater detail than previously possible [1–4].

- (ii) Confinement allows to probe order–disorder phenomena via the sensitivity to boundary conditions [5]. This concept is particularly interesting for two-dimensional crystals, which in a sense are “critical systems” [6–10] throughout the parameter range where crystallinity occurs. Confinement then causes an interesting “crossover” between quasi-one-dimensional [11, 12] behavior and two-dimensional behavior (melting of Kosterlitz–Thouless [6–8] type!). Wall effects then naturally lead to introduce the concept of “surface critical exponents” [13, 15] (Fig. 1.1).
- (iii) Confinement of a crystal naturally may lead to misfits, and the crystal may release its strain by defect formation: our recent simulations [12] have suggested that, as a consequence, soliton staircases [16] may form, and deformation patterns appear which can be interpreted as standing strain waves [12].

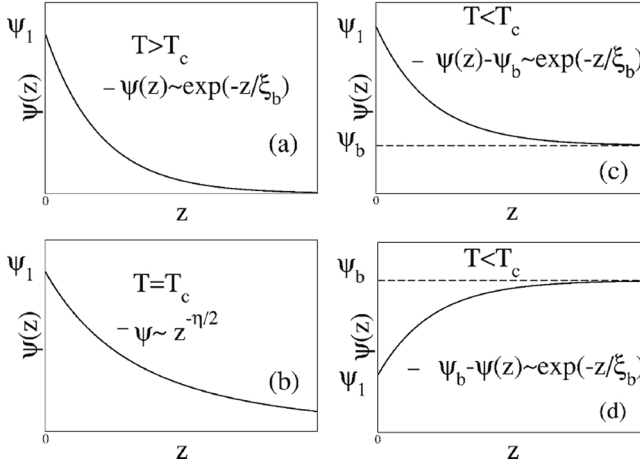


Fig. 1.1 Schematic variation of a local one-component order parameter $\psi(z)$ as a function of the distance z from a wall (or free surface, respectively) that is located at $z = 0$. At temperature $T = T_c$ occurs a second-order phase transition in the bulk (order parameter $\psi_b > 0$ for $T < T_c$). In cases (a)–(c) it is assumed that at the wall at $z = 0$ a local surface field H_1 conjugate to the order parameter $\psi_1 = \psi(z = 0)$ acts. Surface-induced ordering then occurs in a region of order ξ_b (bulk correlation length) for $T > T_c$, while at $T = T_c$ a power-law decay occurs (b), $\psi \propto z^{-\eta/2}$, where η describes the decay of critical correlations in the bulk. Case (d) refers to a “neutral surface” ($H_1 = 0$), assuming a reduction of ordering at the surface (e.g., caused by “missing neighbors”). Also for $T < T_c$ the range over which $\psi(z)$ deviates from ψ_b is given by ξ_b .

1.2 The Simulated Model

An experimental model system for two-dimensional colloidal crystals and their melting behavior is obtained by bringing spherical colloids (diameter in the micrometer range) that contain a superparamagnetic nanoparticle in their core at the water–air interface, orienting the magnetic field perpendicular to the interface, so that a (uniformly) repulsive interaction decaying with distance r as r^{-3} results [17–19]. Varying the strength of the magnetic field, the strength of this interaction can be tuned. This system has become very popular as an experimental model system for the study of melting in $d = 2$ dimensions [20].

Other related $d = 2$ orderings can be prepared in dusty plasmas [21], lattices of spherical block copolymer micelles in thin films [22], superstructures of small molecules or atoms adsorbed on stepped surfaces [23], etc. For this reason, we shall not address a particular physical system, but rather consider a generic model.

Our model consists of point particles in the two-dimensional xy -plane, interacting with the “soft disk” potential which is just the repulsive term of a Lennard-Jones potential

$$V(r) = \varepsilon(\sigma/r)^{12} \quad (1.1)$$

choosing units such that $\varepsilon = 1$ and $\sigma = 1$. In the Monte Carlo simulations, we use a cutoff $r_c = 5\sigma$, because for $r > r_c$, $V(r)$ is completely negligible. Due to this short range of the potential, it is computationally more convenient than the r^{-3} potential, and moreover in the bulk the properties of the model have already been very thoroughly studied [24]; e.g., choosing a density $\rho = 1.05$ it is known that melting (presumably via a KTHNY [6–8] transition) occurs at $T \approx 1.35$ (note that for (1.1) the equation of state does not depend on ρ and T separately, it is only the combination $\rho(\varepsilon/k_B T)^{1/6}$ that matters [25]). So choosing $T = 1$ ensures to obtain states deep in the solid crystalline phase, where the particles form a defect-free triangular lattice structure.

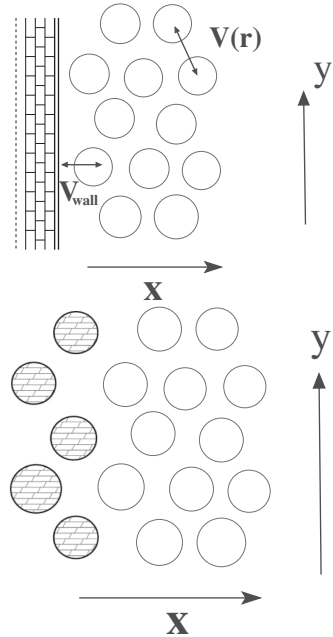
The emphasis of this chapter is to understand the effect of boundaries. Two types of boundaries are considered (Fig. 1.2): so-called structured walls, consisting of two rows of particles frozen in the perfect crystalline order (appropriate for the chosen density). These walls have the proper corrugation in y -direction commensurate with the bulk lattice structure. We are not aware that this type of boundary condition has already been realized in the laboratory (simulation can go beyond experiment!), but for colloids it is perhaps realizable by suitable interference of laser fields: this remains a challenge for the experimentalists.

The other type of wall is provided by a flat structureless boundary, running along the y -direction, and described by another repulsive power law

$$V_{\text{wall}} = \varepsilon_{\text{wall}}(\sigma/x)^{10} \quad (1.2)$$

As described in [5], $\varepsilon_{\text{wall}}$ can be chosen such (namely $\varepsilon_{\text{wall}} = 0.0005$) that the perfect crystalline order in x -direction also remains undisturbed, if the origin

Fig. 1.2 Schematic description of the two types of walls used in this chapter to confine the triangular crystal. Walls are oriented along the y -axis. The *upper part* shows the case of planar walls, the *lower part* shows the case of “structured walls” (cf. text). The frozen particles (*shaded*) interact with the mobile particles (*open circles*) with the same pair potential, (1.1), as acts in the bulk



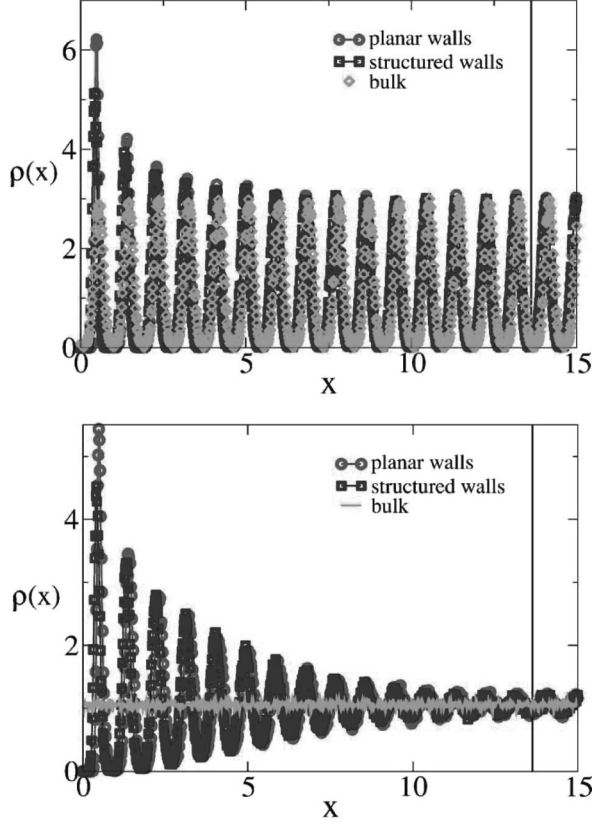
($x = 0$) would coincide with the position of a row of particles in the lattice. We call this type of wall “planar wall.” In both cases, we choose two parallel and identical walls a distance D apart and consider first the case that this distance D is commensurate with the triangular lattice structure, i.e., an integer number n_x of parallel rows of particles fits in between the two walls, with the undisturbed lattice spacing. In the y -direction parallel to the walls, we choose a periodic boundary condition at a distance $L_y = n_y a$, a being the lattice spacing of the triangular lattice.

1.3 Results for Crystals with Commensurate Confinement

Now crystals show two types of long-range order, positional long-range order and orientational long-range order, and the question that we ask is, how are these orderings affected by the presence of walls?

It is easy to see that the positional order in the direction perpendicular to the walls is enhanced, in comparison with the bulk; see the density distributions $\rho(x)$ in the x -direction (Fig. 1.3). This enhancement relative to the bulk occurs for both planar and structured wall boundary conditions, in the solid phase (Fig. 1.3, top). Even in the liquid phase (Fig. 1.3, bottom) there occurs a pronounced layering effect. While the amplitude of this layering near the walls does depend somewhat on the type of boundary condition, the range over which it extends into the bulk is the same for both boundary conditions, as expected (Fig. 1.1) since this range just is a type of bulk correlation length. When one studies the temperature dependence of

Fig. 1.3 Density distribution $\rho(x)$ plotted vs. x for a system of 900 particles in a $D \times L$ geometry, with periodic boundary conditions in the y -direction, $L = n_y a_0$, $D = n_x a_0 \sqrt{3}/2$, with lattice spacing $a_0 = (2/\sqrt{3}\rho)^{1/2} = 1.049$. *Top part* refers to $T = 1.2$ and *bottom part* refers to $T = 1.6$. Only the *left part* of the strip is shown in each case (the center of the strip, $x = D/2$, is marked by a vertical line). A strip with “planar wall” and with “structured wall” boundary condition is included, cf. text, as well as the density distribution of a corresponding bulk system



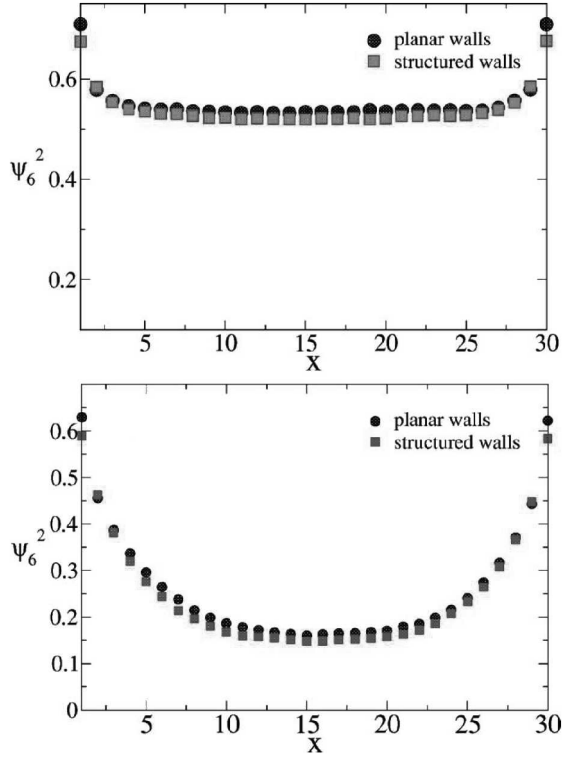
this correlation length in the liquid phase, one finds a pronounced increase as the temperature is lowered toward the melting transition temperature [5], as expected due to the KTHNY [6–8] character of the transition.

Orientational order, appropriate for a triangular lattice, is characterized by local order parameter $\psi_6(\vec{r}_k)$ and associated correlation function $g_6(y)$

$$\psi_6(\vec{r}_k) = (1/6) \sum_{j(\text{n.n. of } k)} \exp(6i\phi_{jk}), \quad g_6(y) = |\langle \psi_6(\vec{r}_k) \psi_6(\vec{r}_\ell) \rangle| \quad (1.3)$$

where $\vec{r}_k = (x_k, y_k)$ is the position of the k th particle and $y = |y_k - y_\ell|$. The angle between a bond connecting particles k and j and a reference direction (e.g., the y -direction) is denoted as ϕ_{jk} . One sums $\exp(6i\phi_{jk})$ over all six nearest neighbors of k , so $\psi_6(\vec{r}_k) = 1$ for a perfect triangular lattice. Also this orientational order is strongly enhanced by the walls (Fig. 1.4), and the orientational correlation length that one can extract from this decay also increases as one approaches melting [5] (the correlation length for orientational order is found to be somewhat larger than its counterpart for positional order (as expected, since it is only the former length

Fig. 1.4 Plot of the local orientational order parameter square $\langle |\psi_6(x)|^2 \rangle$ vs. x for the same system as in Fig. 1.3, for $T = 1.2$ (top part) and $T = 1.6$ (bottom part). Circles refer to the planar wall and square to the structured wall boundary condition



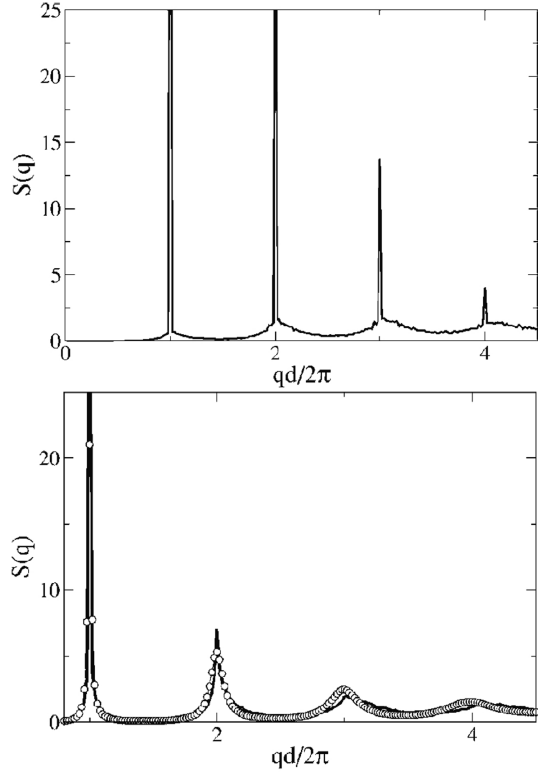
that diverges at the fluid–hexatic transition [7]). From Fig. 1.4 it is clear that for strips of any finite width D the melting transition is strongly affected by finite size rounding: the walls induce a significant orientational order also in the fluid phase, and so the average mean square order parameter $\langle \psi_6^2 \rangle = \int dx \langle |\psi_6(x)|^2 \rangle / D$ decays gradually with increasing temperature and stays nonzero also in the fluid phase for any value $D < \infty$.

In contrast to this enhancement of order due to the walls, seen in Figs. 1.3 and 1.4, a different behavior results when we study the positional order in the y -direction parallel to the walls. Defining for a crystal row in the y -direction the static structure factor $S(q)$, assuming also an orientation of the wavevector \vec{q} along the y -direction, as

$$S(q) = (1/n_y) \sum_{\ell, \ell'} \langle \exp[iq(y_\ell - y_{\ell'})] \rangle \quad (1.4)$$

one obtains at $T = 1$ (i.e., far below the melting temperature) the behavior shown in Fig. 1.5: for structured walls, the expected picture for a crystal indeed results: There are sharp Bragg peaks at the positions $qd/2\pi = 1, 2, 3, \dots$, with $d = a_0$ now, distinct from the background (“thermal diffusive scattering”). As expected, the height of these peaks decreases with increasing q , due to the effect of the Debye–Waller

Fig. 1.5 Static structure factor $S(q)$ at $T = 1$ plotted vs. $qd/2\pi$ for structured walls (*top part*) and for planar walls (*bottom part*). All data are for systems with $n_x = 30$ rows and $n_y = 100$ particles per row along the y -direction, and the data were averaged over all rows. For the planar walls the full curve is a fit to (1.5)



factor [16]. The width of these Bragg peaks does not increase with increasing q , as it should be.

In contrast, for planar walls the structure factor behaves qualitatively different; it looks similar like a fluid structure factor: only the first peak is very high and rather sharp, but the higher order peaks (at $qd/2\pi = 2, 3, \dots$) are systematically broadened. In this case $S(q)$ is in almost quantitative agreement with the theoretical result for a one-dimensional harmonic chain [11]

$$S(q) = \sinh(q^2 \delta^2 / 2) [\cosh(q^2 \delta^2 / 2) - \cos(qd)] \quad (1.5)$$

with Hamiltonian

$$\mathcal{H} = \frac{1}{2} \sum_{\ell} \left[\pi_{\ell}^2 / m + mc^2 (y_{\ell+1} - y_{\ell} - d)^2 / d^2 \right] \quad (1.6)$$

where point particles of mass m have positions y_{ℓ} and conjugate momenta π_{ℓ} . In the classical ground state one has a one-dimensional crystal, particles residing at positions $y_n = y_0 + nd$, $n = 1, 2, \dots, d$, being the lattice spacing. The parameter c plays the role of a sound velocity. From (1.6) it is straightforward to compute the

displacement correlation function

$$\langle (u_n - u_0)^2 \rangle = n\delta^2, \quad \delta = a\sqrt{k_B T / (mc^2)} \quad (1.7)$$

Equations (1.5) and (1.7) imply that a one-dimensional crystal melts continuously at $T = 0$, and as $T \rightarrow 0$ the correlation length $\xi = a^3 / (2\pi\delta^2) \propto 1/T \rightarrow \infty$ as $T \rightarrow 0$ [5, 11].

The different character of the lateral order (in the y -direction) for systems with planar walls is evident when one compares snapshot pictures of superimposed configurations (Fig. 1.6). For the structured wall case, the triangular lattice structure is nicely recognized. The size of the irregular dots measures the mean square displacement of the particles around the lattice sites. Clearly these displacements are smaller near the structured wall – the effective periodic potential created by such a wall enhances order.

The situation is very different for the planar wall case, however: the displacement distributions of the particles around the lattice positions now are very anisotropic, indicating a pronounced softness of the system along the y -direction. This behavior is reminiscent of a two-dimensional smectic phase, and it shows up also in the behavior of the elastic constants (Fig. 1.7). For a perfect triangular crystal structure, in the bulk, the symmetry relations $C_{11} = C_{22}$ and $C_{12} = C_{33}$ hold (we use here the Voigt notation for the elastic constants). This symmetry is broken in a strip of finite width due to the walls, but increasing the width $D = na_0\sqrt{3}/2$ one finds a rapid convergence toward bulk for planar walls: while C_{11} , C_{22} , C_{12} converge to bulk behavior, C_{33} does not, and rather $C_{33}(n) = C_{33}^{\text{bulk}}/2$, apparently independent of the number n of rows in the strip! Since the elastic moduli in the bulk are $C_{22} \approx 127$, $C_{33} \approx 41$ (in units of $k_B T / \sigma^2$), and the pressure is $p = 17.5$, the shear modulus $\mu = C_{33} - p$ in the strip vanishes (at least approximately). The planar boundaries provide an elastic distortion of long range to the crystal and hence modify the crystalline behavior significantly.

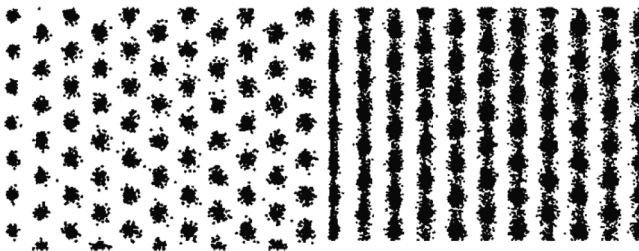
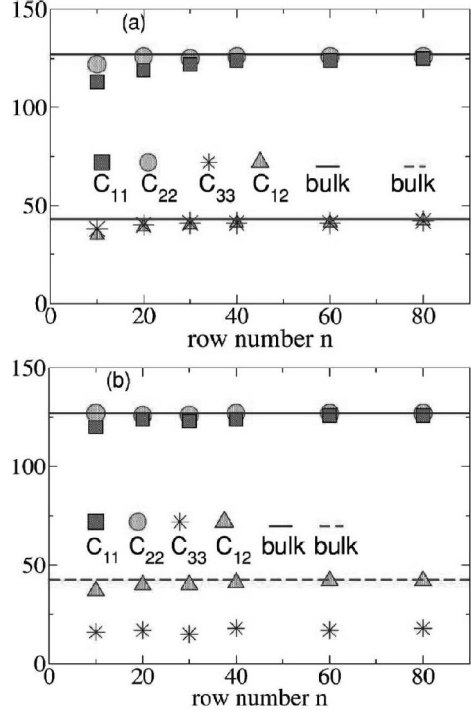


Fig. 1.6 Configuration of the particles in the first nine rows adjacent to the left wall at $T = 1.0$, for the structured wall (*left*) and the planar wall (*right*). One thousand configurations of a run lasting 10^6 Monte Carlo steps per particle are superimposed, fixing the center of mass of the total system of mobile particles in each configuration in the same position. A system with $n_x = 30$ rows and $n_y = 30$ particles per row was used, with periodic boundary conditions in the y -direction

Fig. 1.7 Elastic constants (in units of $k_B T / \sigma^2$) for systems at $k_B T / \varepsilon = 1.0$ for structured walls (*top part*) and planar walls (*bottom part*).

Horizontal straight lines show the bulk values, obtained for a system with periodic boundary conditions in both x - and y -directions



1.4 Insight Gained from the Harmonic Theory of Two-Dimensional Crystals

In order to better understand the anomalous behavior of crystalline strips with planar walls, it is useful to examine the mean square displacement correlation function in the y -direction, $G(y) = \langle |u_y(y) - u_y(0)|^2 \rangle$, where $\vec{u} = (u_x, u_y)$ is the displacement vector of a particle relative to its position in the perfect triangular lattice. Choosing for simplicity a $D \times L$ geometry with periodic boundary conditions also in the x -direction, one finds $\{\vec{Q} = (Q_x, Q_y)\}$

$$\langle [u_y(y) - u_y(0)]^2 \rangle = (2/N) \sum_{Q_x} \sum_{Q_y} \langle u_y(\vec{Q}) u_y(-\vec{Q}) \rangle [1 - \cos(y Q_y)] \quad (1.8)$$

where Q_x, Q_y are “quantized” as follows:

$$Q_x/\pi = -1, -1 + \frac{2}{D}, -1 + \frac{4}{D}, \dots, +1 - \frac{2}{D} \quad (1.9)$$

$$Q_y/\pi = -1, -1 + \frac{2}{L}, -1 + \frac{4}{L}, \dots, +1 - \frac{2}{L} \quad (1.10)$$

Using the continuum approximation for a two-dimensional harmonic solid [16], the correlator in (1.8) becomes [16]

$$\langle u_\alpha(\vec{Q}) u_\beta(-\vec{Q}) \rangle = \frac{k_B T / Q^2}{(\lambda + 2\mu - p)} \hat{Q}_\alpha \hat{Q}_\beta + \frac{k_B T / Q^2}{\mu - p} (\delta_{\alpha\beta} - \hat{Q}_\alpha \hat{Q}_\beta) \quad (1.11)$$

where $\hat{Q}_\alpha = Q_\alpha / |\vec{Q}|$ is the Cartesian component ($\alpha = x, y$) of a unit vector in the direction of \vec{Q} , and the Lamé coefficient $\lambda = (C_{11} - C_{33})/2$ ($=42$, for $k_B T / \varepsilon = 1$ in our model).

Since all parameters in (1.8), (1.9), (1.10), and (1.11) are hence explicitly known for the present model, (1.8) can straightforwardly be evaluated numerically (Fig. 1.8). On the other hand, in the limit $a_0 \ll D \ll L$ one can convert the sum over Q_y into an integral and thus obtain analytical results approximately, to show that then a crossover from a two-dimensional behavior to the one-dimensional behavior (1.7) occurs,

$$G(y) \propto \ln y, \quad a_0 \ll y \ll D \ln D \quad (\text{two dimensions}) \quad (1.12)$$

$$G(y) \propto y, \quad D \ln D \ll y \ll L \quad (\text{one dimension}) \quad (1.13)$$

Using the results obtained for μ , λ , and p from the simulation, we have worked out (1.8) for $D = 20a_0\sqrt{3}/2$, $L = 500a_0$, i.e., the largest system for which we have also carried out a Monte Carlo simulation (Fig. 1.8). The results show that for $y \leq 40$ indeed a logarithmic increase of $G(y)$ is compatible with the data, as expected from (1.12). For $y > 40$, a faster increase sets in (but it is difficult to numerically verify (1.13), since the periodic boundary condition, $G(y) = G(L - y)$,

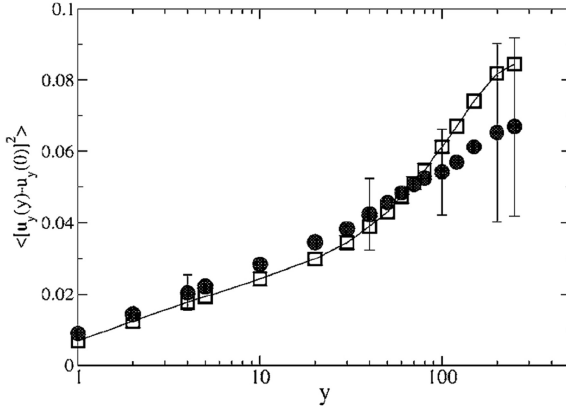


Fig. 1.8 Comparison of $G(y)$ according to the harmonic theory ((1.8), (1.9), (1.10), and (1.11), squares) and corresponding Monte Carlo data (full dots with error bars), for a system with $n_x = 20$ rows containing $n_y = 500$ particles each. $G(y)$ is given in units of σ^2 ($\sigma = 1$). Periodic boundary conditions are used in both the x - and y -directions. Note the logarithmic scale of the abscissa, while the ordinate has a linear scale

reduces the increase of $G(y)$ already for $y \approx L/4$ [5]). Moreover, the results from the numerical implementation of the harmonic theory are in almost perfect quantitative agreement with the Monte Carlo data, implying that at the chosen temperature (far below melting) anharmonic effects still are insignificant.

This quasi-one-dimensional behavior of elongated two-dimensional strips is only one ingredient to understand the anomalous behavior of crystalline strips confined by planar walls: the other ingredients are critical surface effects. One finds that in the region where the logarithmic increase $G(y)$ with y occurs, the prefactor of this increase is about a factor of 2 larger for rows adjacent to a wall than for rows in the bulk (Fig. 1.9). Actually this behavior is expected by analogy with the two-dimensional XY -model [6, 15, 26]. Remember that a two-dimensional crystal is a critical system, where there is no true positional long-range order [7–10], but rather a power-law decay of a suitably defined correlation function. To remind the reader of this analogy and clarify what it implies for correlations near free surfaces [15, 26], we approximate the XY -model as

$$\mathcal{H}_{xy} = -J \sum_{\ell, j} \cos(\phi_\ell - \phi_j) \approx \frac{1}{2} J \sum_{\langle \ell, j \rangle} (\phi_\ell - \phi_j)^2 \quad (1.14)$$

Here J is the exchange constant, and we have a lattice (site j) where unit vectors occur, characterized by their orientation angle ϕ_j relative to the y -axis in the xy -plane. The quantity of interest is the spin correlation function

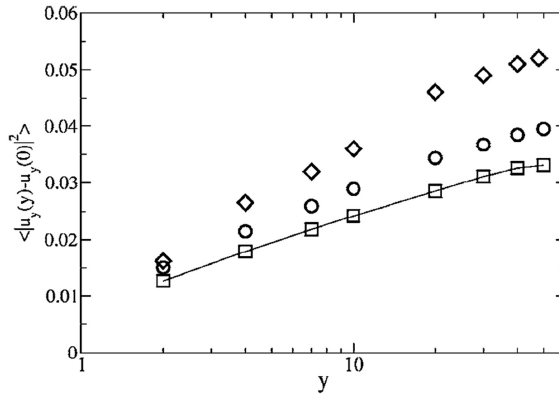


Fig. 1.9 Plot of $G(y)$ vs. y (logarithmic scale!) for two-dimensional crystalline strips at $k_B T/\varepsilon = 1.0$ and $n_x = 20$ rows containing $n_y = 100$ particles each. *Squares* show the prediction of the corresponding harmonic theory of a bulk system, while *circles* and *diamonds* are Monte Carlo data. *Circles* show data for a system with periodic boundary conditions, while *diamonds* show data for a system with planar walls, using only the displacement of particles adjacent to the walls. $G(y)$ is given in units of σ^2 ($\sigma = 1$)

$$g(\vec{r}) = \langle \vec{S}(\vec{r}_0) \cdot \vec{S}(\vec{r}_0 + \vec{r}) \rangle = \langle \cos[\phi(\vec{r} + \vec{r}_0) - \phi(\vec{r}_0)] \rangle \\ \approx \exp \left\{ -\frac{1}{2} \langle [\phi(\vec{r} + \vec{r}_0) - \phi(\vec{r}_0)]^2 \rangle \right\} \quad (1.15)$$

Equations (1.14) and (1.15) make the analogy to harmonic solids transparent – the angles $\{\phi_j\}$ correspond to the displacement vectors \vec{u}_j and $\langle [\phi(\vec{r} + \vec{r}_0) - \phi(\vec{r}_0)]^2 \rangle$ corresponds to the displacement correlation $G(y)$. Now the well-known power-law decay of $g(\vec{r})$, $g(r) \propto r^{-\eta_b}$, immediately follows from a logarithmic variation of the angular displacement correlation

$$\langle [\phi(\vec{r} + \vec{r}_0) - \phi(\vec{r}_0)]^2 \rangle = (k_B T / 2\pi J) \ln(\pi r / a_0), \quad r \gg a_0 \quad (1.16)$$

which yields $\eta_b = k_B T / (2\pi J)$. Equation (1.16) is the analog of (1.12).

When one introduces the continuum approximation that corresponds to (1.14) namely

$$\mathcal{H} = \frac{J}{2} \int [\nabla \phi]^2 dx dy \quad (1.17)$$

one can treat the problem of a semiinfinite half-space (with a free boundary at $x = 0$) by postulating a von Neumann boundary condition

$$\partial G(\vec{r}_1, \vec{r}_2) / \partial x_1 |_{x_1=0} = 0 \quad (1.18)$$

for the correlation function $G(\vec{r}_1, \vec{r}_2) = \langle \phi(\vec{r}_1) \phi(\vec{r}_2) \rangle$. Using (1.17) and (1.18) one can show [26] that

$$\langle \exp[i\phi(\vec{r}_1)] \exp[i\phi(\vec{r}_2)] \rangle \propto (y_2 - y_1)^{-\eta_{||}}, \quad \eta_{||} = 2\eta_b \quad (1.19)$$

when both sites \vec{r}_1, \vec{r}_2 lie at the surface ($x_1 = x_2 = 0$), η_b being the exponent quoted in (1.16). When only one site is in the surface, while the other site is deep in the bulk, one rather predicts a power law $g(x) \propto x^{-\eta_{\perp}}$, where scaling [27] yields $\eta_{\perp} = 3\eta_b/2$. While there are no data available to test the latter relation, Fig. 1.9 provides a test for the analog of the relation $n_{||} = 2\eta_b$ for the surface behavior of the displacement correlation of a solid.

1.5 Effects due to Incommensurate Confinement: Soliton Staircases and Strain Density Waves

We now focus on the case where the confinement creates a misfit in the system [12], such that we still have a total number of $N = n_x n_y$ particles, with a linear dimension $L_y = n_y a$ where a is the lattice spacing appropriate for an ideal, undistorted triangular lattice, with periodic boundary conditions in the y -direction, but the thickness D of the strip no longer has the commensurate value $D = n_x (a\sqrt{3}/2)$ but rather

$D = (n_x - \Delta)a\sqrt{3}/2$. Note that in the case of structured walls, the commensurate confinement is achieved by putting the two rows of fixed particles that are just adjacent to the rows of mobile particles at a distance $D' = (n_x + 1)(a\sqrt{3}/2)$, of course; now this distance rather is $D' = (n_x + 1 - \Delta)(a\sqrt{3}/2)$.

When we start the system at $\Delta = 0$ and increase Δ in small steps ($\Delta = 0.25$), equilibrating at each value of Δ the system carefully before increasing Δ further, we can monitor the stress–strain characteristics of the system (Fig. 1.10). As expected, for $\Delta = 0$ the crystal is stress free, and for $\Delta > 0$ the stress increases linearly with Δ . At $\Delta = 2.0$ we observe a jump in the stress–strain curve, where the stress suddenly decreases strongly: inspection of the system configuration reveals that a transition $n_x \rightarrow n_x - 1$ in the number of rows parallel to the confining boundaries

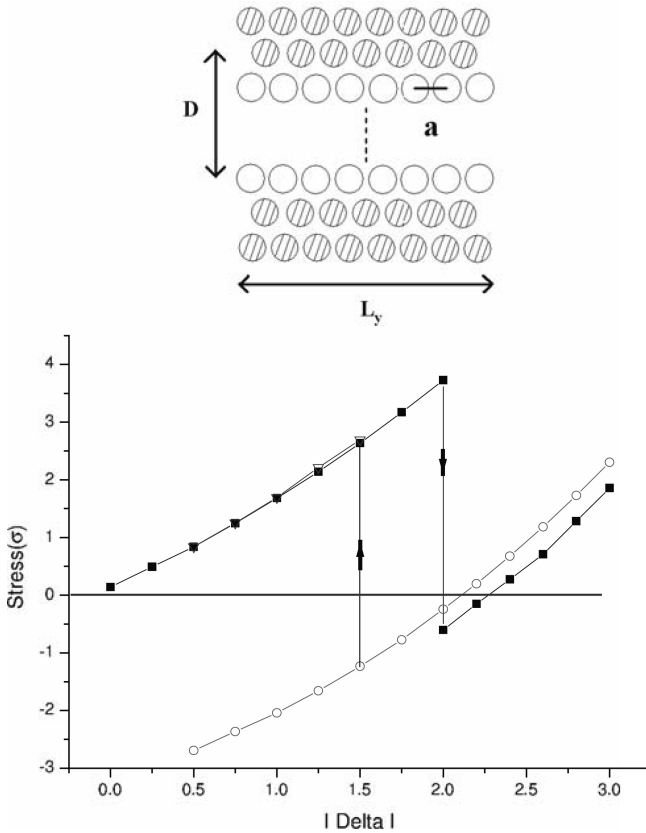


Fig. 1.10 Internal stress $\sigma = \sigma_{yy} - \sigma_{xx}$ (in Lennard-Jones units) at $k_B T/\varepsilon = 1.0$ in the confined crystalline strip plotted vs. Δ , for the case of a system started with $n_x = 30$, $n_y = 108$ (full symbols) and a system started with $n_x = 29$, $n_y = 108$ (plus the 108 extra particles appropriately distributed in the 29 rows, as described in the text (open symbols)). Curves are guides to the eye only. The upper insert shows a schematic sketch of the geometry, the frozen particles being shown as shaded circles, mobile particles are not shaded

has occurred. The n_y particles contained in the row that has disappeared have to be redistributed over the remaining $n_x - 1$ rows, and thus these rows now contain over the distance L_y more than n_y particles (on average). However, the structured wall boundary condition still provides a corrugation potential with a periodicity of the lattice spacing a (corresponding to n_y particles over a distance L_y). As a result, the lattice of the crystal with $n_x - 1$ rows no longer is commensurate with the corrugated boundary potential provided by the “structured walls” [12].

It turns out that (for $k_B T/\varepsilon \leq 1.0$) it is too energetically unfavorable to put any of the n_y extra particles into the two rows immediately adjacent to the frozen particles, while extra particles can occur in all the $(n_x - 3)$ inner rows of the strip. If we assume that the same number of extra particles should occur in any of these rows, we conclude that on average every inner row has $n_d = n_y/(n_x - 3)$ extra particles, and hence the average lattice spacing in the y -direction now is $a' = an_y/(n_y + n_d) = a(n_x - 3)/(n_x - 2)$.

However, due to the corrugation potentials at the confining walls, the strip does not simply adapt the structure of a (distorted) triangular lattice with uniform lattice spacing a' in y -direction: while such a uniform periodicity with lattice spacing a' is indeed found in the center of the strip, near the confining boundaries a more complicated pattern emerges (Fig. 1.11), namely a “soliton staircase” containing n_d steps. This pattern is evident both from superimposed configuration snapshots (Fig. 1.11) and from strain patterns (Fig. 1.12). The strain $u_{ij} = \partial u_i/\partial x_j + \partial u_j/\partial x_i$ is calculated from the particle configurations, where $u_i(\vec{R}_n)$ is the i -component of the displacement vector of the particle labeled by n relative to the site \vec{R}_n of the reference lattice and x_i stand for the (two-dimensional) Cartesian coordinates x, y [12].

Note that the pattern of the soliton adjacent to the boundaries resulting from the transition typically exhibits some irregularity. Studying the kinetics of this transition

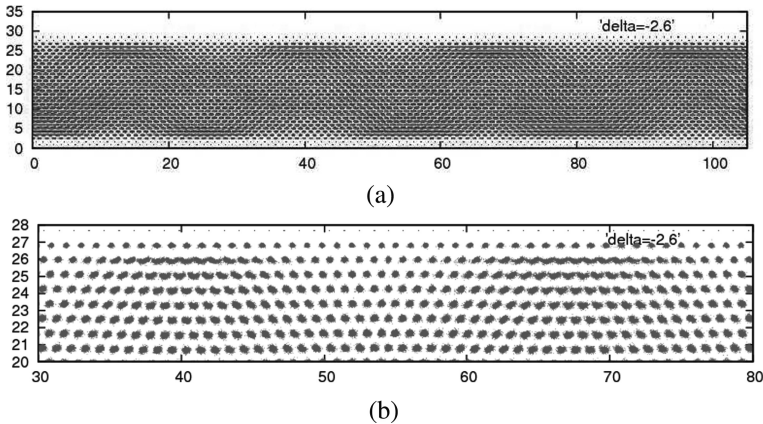


Fig. 1.11 Particle configuration in a system with $n_x = 30$, $n_y = 108$, $\Delta = 2.6$, where a transition $n_x \rightarrow n_x - 1$ has occurred, at a temperature $k_B T/\varepsilon = 1.0$. (a) 750 superimposed positions of the particles and (b) close-up of the structure near the upper wall. Numbers shown along the axes indicate the Cartesian coordinates of the particles

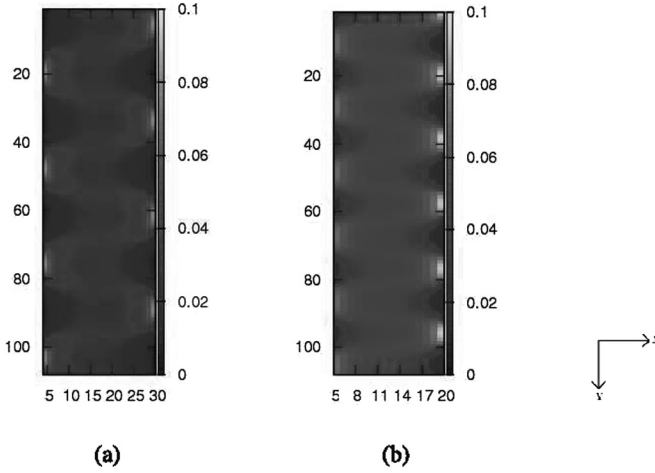


Fig. 1.12 Strain patterns of a system at $k_B T / \varepsilon = 0.1$ for (a) $n_y = 108, n_x = 30$ and (b) $n_y = 108, n_x = 20$. The calibration bars are shown on the right-hand side of the graphs, and the orientation of the coordinate axes is indicated at the right side

[28] $n_x \rightarrow n_x - 1$ one finds that defects need to be nucleated one by one, and hence a time-consuming equilibration process is needed to generate an (approximately) periodic arrangement of the defects (solitons) along the y -direction (note that at nonzero temperature anyway we must expect large thermal fluctuations of these defects around their average positions). In fact, sometimes states are formed where the number of defects n_d deviates from the theoretical value as estimated above. Presumably these are metastable configurations, separated by (large) barriers from the equilibrium behavior.

Therefore, we have artificially prepared [12] other initial states, where for a given misfit Δ we put $n_y + n_d$ particles in the $n_x - 3$ inner rows, with the n_d excess particles in each of these rows initially at random positions. Indeed we find that this way of preparation of the system leads to a much more regular pattern of the resulting strain density waves (Fig. 1.12).

The periodicity of the soliton staircase shows up very nicely when one studies the Lindemann parameter $\ell(n)$ defined as $\langle u_x^2(\vec{R}_n) \rangle - \langle u_x(\vec{R}_n) \rangle^2$ [12] but this shall not be further elaborated here. However, we emphasize that by such confinement of crystals with boundaries that create misfit we can create a superstructure (via the wavelength of the strain density wave pattern) which is of the same order as the thickness of the strip.

1.6 Conclusions

In this brief review, confinement of two-dimensional crystals in strip geometry was considered, based on Monte Carlo simulations of a generic model and pertinent theoretical considerations. It was argued that the confinement has particularly dramatic

effects on the ordering, given the fact that a two-dimensional crystal is a “critical system” (lack of positional long-range order, possibility that melting happens according to the KTHNY scenario).

Assuming a confinement that is commensurate with the crystal structure, it was shown that confinement enhances the positional order in the direction perpendicular to the boundary (“layering”) and that orientational order parallel to the boundary always gets enhanced. However, positional order parallel to the flat boundary (“planar wall”) gets weakened or even destroyed. Both the crossover to quasi-one-dimensional behavior of strips of finite width and surface critical behavior contribute to these effects, and the shear elastic constant of the strip was found to be (almost) zero.

Particularly interesting are compressed strips, where transitions occur from n to $n - 1$ rows parallel to the walls. The “structured wall” boundary condition then implies incommensurability with the periodicity of the film, leading to the formation of “soliton staircases” along the boundaries, and the solitons act as cores of standing strain waves in the system.

While the original motivation of this research stems from colloidal crystals [17–20], we emphasize that related phenomena could occur in very different systems, e.g., various semiconductor devices such as quantum dot superlattices [29], lattice-mismatched fused GaAs/In P wafers [30], $\text{Ge}_x\text{Si}_{1-x}$ /Si heterostructures [31], and rotationally misaligned Si wafers covalently bonded together [32]. In all such systems boundary-induced strain fields can occur. A particularly nice example where the misfit between a crystal and a frozen boundary can be controlled by external magnetic field is superconducting vortex lattices [33]. A very interesting aspect, closely related to the work reviewed here but out of scope of this chapter, is unconventional nonlinear mechanical response properties of confined solids [34, 35]. Thus, we feel that the phenomena described in the present brief review should have widespread applications in the physics of condensed matter.

Acknowledgments This research was partially supported by the Deutsche Forschungsgemeinschaft (DFG), Project TR 6/C4.

References

1. W.C. Poon, P.N. Pusey, in: *Observation, Prediction and Simulation of Phase Transitions in Complex Fluids*, ed. by M. Baus, F. Rull, J.P. Ryckaert (Kluwer, Dordrecht, 1995) p. 3
2. T. Palberg, Colloidal crystallisation dynamics. *Curr. Opin. Colloid Interface Sci* **2**, 607 (1997)
3. H. Löwen, Colloidal soft matter under external control. *J. Phys.: Condens. Matter* **13**, R415 (2001)
4. W.C. Poon, Colloids as big atoms. *Science* **304**, 830 (2004)
5. A. Ricci, P. Nielaba, S. Sengupta, K. Binder, Ordering of two-dimensional crystals confined in strips of finite width. *Phys. Rev. E* **75**, 011405 (2007)
6. J.M. Kosterlitz, D.J. Thouless, Ordering, metastability and phase transitions in two-dimensional systems. *J. Phys. C* **6**, 1181 (1973)

7. B.I. Halperin, D.R. Nelson, Dislocation-mediated melting in two dimensions. *Phys. Rev.* **B19**, 2457 (1979)
8. A.P. Young, Melting and the vector Coulomb gas in two dimensions. *Phys. Rev.* **B19**, 1855 (1979)
9. B. Jancovici, Infinite susceptibility without long-range order: the two-dimensional harmonic "solid". *Phys. Lett.* **19**, 20 (1967)
10. N.D. Mermin, Crystalline order in two dimensions. *Phys. Rev.* **176**, 250 (1968)
11. V.J. Emery, J.D. Axe, One-dimensional fluctuations and the chain-ordering transformation in Hg_3AsF_6 . *Phys. Rev. Lett.* **40**, 1507 (1978)
12. Y.-H. Chui, S. Sengupta, K. Binder, Soliton staircases and standing strain waves in confined colloidal crystals. *EPL* **83**, 58004 (2008)
13. K. Binder, P.C. Hohenberg, Phase transitions and static spin correlations in ising models with free surfaces. *Phys. Rev.* **B6**, 3461 (1972)
14. K. Binder, P.C. Hohenberg, Surface effects on magnetic phase transitions. *Phys. Rev.* **B9**, 2194 (1974)
15. B. Berche, Bulk and surface properties in the critical phase of the two-dimensional XY model. *J. Phys.* **A36**, 585 (2003)
16. P.M. Chaikin, T. C. Lubensky, *Principles of Condensed Matter Physics* (Cambridge University Press, Cambridge, MA, 1995)
17. K. Zahn, R. Lenke, G. Maret, Two-stage melting of paramagnetic colloidal crystals in two dimensions. *Phys. Rev. Lett.* **82**, 2721 (1999)
18. K. Zahn, G. Maret, Dynamic criteria of melting in two dimensions. *Phys. Rev. Lett.* **85**, 3656 (2000)
19. M. Köppl, P. Henseler, A. Erbe, P. Nielaba, P. Leiderer, Layer reduction in driven 2D-colloidal systems through microchannels. *Phys. Rev. Lett.* **97**, 208302 (2006)
20. C. Eisenmann, P. Keim, U. Gasser, G. Maret, Melting of anisotropic colloidal crystals in two dimensions. *J. Phys., Condens. Matter*, **16**, S4095 (2004)
21. L.-W. Teng, P.-S. Lu, I. Lin, Microscopic observation of confinement-induced layering and slow dynamics of dusty-plasma liquids in narrow channels. *Phys. Rev. Lett.* **90**, 245004 (2003)
22. R.A. Segalman, A. Hexemer, E.J. Kramer, Edge effects on the order and freezing of a 2D array of block copolymer spheres. *Phys. Rev. Lett.* **91**, 196101 (2003)
23. K. Binder, in *Cohesion and Structure of Surfaces, Ch. III*, ed. by D.G. Pettifor (Elsevier, Amsterdam, 1995), p. 121
24. K. Bagchi, H.C. Andersen, W. Swope, Observation of a two-stage melting transition in two dimensions. *Phys. Rev. E* **53**, 3794 (1996)
25. J.P. Hansen, I.R. McDonald, *Theory of Simple Liquids* (Academic, London, 1986)
26. J.L. Cardy, Conformal invariance and surface critical behavior. *Nucl. Phys.* **B240**, 514 (1984)
27. K. Binder, in *Phase Transitions and Critical Phenomena, Vol 8*, ed. by C. Domb and J.L. Lebowitz (Academic, New York, NY, 1983) p.1
28. Y.-H. Chui, S. Sengupta, I.M. Snook, K. Binder, The observation of formation and annihilation of solitons and standing strain wave superstructures in a two-dimensional colloidal crystal. *J. Chem. Phys.* **132**, 074701 (2010)
29. E. Sarigiannidou, E. Monroy, B. Daudin, J.L. Rouvière, A.D. Andreev, Strain distribution in GaN/AlN quantum-dot superlattices. *Appl. Phys. Lett.* **87**, 203112 (2005)
30. Z.L. Liao, Strained interface of lattice-mismatched wafer fusion. *Phys. Rev.* **B55**, 12899 (1997)
31. D.D. Prević, B. Bahierathan, H. Lafontaine, D.C. Houghton, D.W. Mc Comb, Kinetic critical thickness for surface wave instability vs. misfit dislocation formation in $\text{Ge}_x\text{Si}_{1-x}/\text{Si}$ (100) heterostructures. *Physica A* **239**, 11(1997)
32. M. Nielsen, B.O. Poulson, C. Kumpf, F. Feidenhans, R.L. Johnson, F. Jensen, F. Grey, Mapping strain fields in ultrathin bonded Si wafers by x-ray scattering. *Appl. Phys. Lett.* **80**, 3412 (2002)

33. R. Bessling, R. Niggebrugge, P.H. Kes, Transport properties of vortices in easy flow channels: a Frenkel-Kontorova study, *Phys. Rev. Lett.* **82**, 3144 (1999); N. Kokubo, R. Besseling, V.M. Vinokur, P.H. Kes, Model locking of vortex matter driven through mesoscopic channels. *Phys. Rev. Lett.* **88**, 247004 (2002)
34. D. Chaudhuri, S. Sengupta, Anomalous structural and mechanical properties of solids confined in quasi-one-dimensional strips. *J. Chem. Phys.* **128**, 194702 (2008)
35. D. Chaudhuri, S. Sengupta, Constrained deformation of a confined solid: anomalous failure by nucleation of smectic bands. *Phys. Rev. Lett.* **93**, 115702 (2004)

Nanophenomena at Surfaces

Fundamentals of Exotic Condensed Matter Properties

Michailov, M. (Ed.)

2011, XX, 284 p., Hardcover

ISBN: 978-3-642-16509-2